

¹ 3DQLayers: Volumetric Layer Based Analysis for Quantitative Renal MRI

³ Alexander J Daniel  ^{1,¶} and Susan T Francis  ^{1,2}

⁴ 1 Sir Peter Mansfield Imaging Centre, University of Nottingham, Nottingham, United Kingdom 2 NIHR
⁵ Nottingham Biomedical Research Centre, Nottingham University Hospitals NHS Trust and the University
⁶ of Nottingham, Nottingham, United Kingdom ¶ Corresponding author

DOI: [10.xxxxxx/draft](https://doi.org/10.xxxxxx/draft)

Software

- [Review](#) 
- [Repository](#) 
- [Archive](#) 

Editor: [Open Journals](#) 

Reviewers:

- [@openjournals](#)

Submitted: 01 January 1970

Published: unpublished

License

Authors of papers retain copyright and release the work under a Creative Commons Attribution 4.0 International License ([CC BY 4.0](#)).

⁷ Summary

⁸ Quantitative Magnetic Resonance Imaging (qMRI) provides informative measurements of ⁹ structure and function of an organ where each volumetric pixel (voxel) provides a measure ¹⁰ of the physical properties of the underlying tissue. Traditionally, analysis of MR images ¹¹ is performed by first segmenting the organ and its constituent tissue types, which for the ¹² kidneys involves separating them into the cortex and medulla, before calculating the average ¹³ measurement within each tissue. The process of segmenting renal tissue types is typically ¹⁴ manual, making it time consuming and prone to inaccuracies.

¹⁵ An alternative to voxel-based analysis in MRI is the layer model which divides the organ into ¹⁶ ordered surfaces. For the kidney, this involves generating layers based on the distance of each ¹⁷ voxel between the outer and inner surface of the kidney. From this, the gradient of change in ¹⁸ qMRI measures between the cortex and medulla of the kidney can be computed to evaluate ¹⁹ pathological and physiological aspects of the kidney. Here, 3DQLayers an open-source Python ²⁰ software package to automatically define and interrogate 3D renal layers is presented.

²¹ Statement of need

²² Background

²³ The kidneys are structurally and functionally complex organs in the abdomen responsible for ²⁴ the removal of waste products and excess fluid from the blood to produce urine ([Lote, 2012](#)). ²⁵ Each kidney is separated into the cortex which forms the outer layer of the kidney and the ²⁶ medulla in the inner part which is arranged in a series of small pyramids ([Hall, 2015](#)), as shown ²⁷ in [Figure 1](#). The kidney maintains homeostasis through filtration, reabsorption, secretion, and ²⁸ maintenance of the cortico-medullary gradient (CMG), meaning a method to assess changes in ²⁹ physiology from the cortex to the medulla is key.

³⁰ Conventional MRI primarily assesses signal intensity in a voxel in arbitrary units, however ³¹ Quantitative MRI (qMRI) goes beyond conventional MRI by instead providing voxel-wise ³² measurements with numerical significance in physical units, based on the tissues underlying ³³ properties. For example, qMRI of relaxation times with parameters which carry information ³⁴ about the local microstructure, or those of how readily water can diffuse through the tissue ³⁵ and the rate at which blood perfuses the tissue. To interpret quantitative images, regions of ³⁶ interest (ROIs) for the kidney cortex and medulla are defined and statistical analysis performed ³⁷ on the voxels within each ROI. Segmenting such ROIs manually is time consuming, and prone ³⁸ to intra- and inter-reader variation.

³⁹ The group of Pruijm proposed an alternative to voxel based ROI analysis of tissue termed ⁴⁰ the Twelve Layer Concentric Object (TLCO) method ([Li et al., 2020](#); [Milani et al., 2017](#);

41 Piskunowicz et al., 2015) where users delineate the inner and outer boundaries of the kidney
42 to generate twelve equidistant layers between the renal pelvis and the surface of the kidney.
43 The outer layers represent the cortex and the inner layers the medulla, with the gradient across
44 the central layers computed to estimate the CMG. Since this layer-based analysis only requires
45 segmentation of the boundaries of the kidney, rather than the cortex and medulla within, it
46 is quicker and more repeatable. An analogy to this is the development of the layer-based
47 analysis tools applied in the brain for neuroimaging including BrainVoyager (Goebel, 2012),
48 CBSTools/Nighres (Bazin et al., 2014; J. Huntenburg et al., 2017; J. M. Huntenburg et al.,
49 2018), FreeSurfer (Fischl, 2012), and FSL (Jenkinson et al., 2012).

50 However, the TLCO software is closed-source and has some limitations. It requires manual
51 delineation of the outside and inside surfaces of the kidney, divides the kidney into the same
52 number of layers irrespective of the size of the kidney, and can only be performed on a single
53 slice cutting through the kidneys on their longest axis (coronal-oblique) which is not always
54 desirable (Bane et al., 2020). Due to the spatial distribution of kidney pathology, there is a
55 need to acquire multi-slice images for full 3D coverage of the kidney to increase the number of
56 voxels sampled and gain a better understanding of the heterogeneity of the kidney. Recently,
57 an automated-TLCO method has been proposed (Ishikawa et al., 2022) to determine the CMG
58 from the water signal of a Dixon scan, however this work again has limitations of not being
59 full kidney coverage, including the renal pelvis, and highlights the difficulty in analysing small
60 kidneys with a fixed number of layers.

61 The motivation of 3DQLayers was to address these limitations of TLCO to provide an open-
62 source Python package to automatically define 3D, multi-slice layers in the kidney of known
63 thickness for quantitative-depth based analysis across a range of kidney MRI data, enabling its
64 use in large renal MRI trials to address clinical questions.

65 Methods

66 3DQLayers is an open-source Python package building on the ideas within TLCO, with the
67 fundamental difference that the layers are defined based on a voxels' distance from the surface
68 of the kidney in millimetres rather than the proportion of the kidney. As such, the input to
69 3DQLayers is a whole kidney mask, which can be automatically generated from a structural
70 image (e.g. here using a U-net applied to T₂-weighted images (Daniel et al., 2021; Daniel,
71 2024)).

72 The pipeline for defining the layers from the whole kidney mask is outlined in Figure 2. Pre-
73 processing steps first fill in the holes in the kidney mask caused by cysts, as the surface of a
74 cyst is not characteristic of the surface of the kidney. Next, the voxel-based representation of
75 the mask is converted to a smoothed mesh-based representation of the kidneys, the distance
76 from the centre of each voxel to the surface of the mesh is calculated to produce a depth
77 map (Dawson-Haggerty, 2023). Tissue adjacent to the renal pelvis that is not representative
78 of the medulla is then excluded from layer-based analysis. This is achieved by automatically
79 segmenting the renal pelvis then calculating the distance from each voxel to the renal pelvis as
80 described above. Those voxels closer than a specified threshold, typically 10 mm, are excluded
81 from the depth map. Finally, a layer image is generated by quantising the depth map to a
82 desired layer thickness, typically 1 mm.

83 The layer image and quantitative images are resampled to the same spatial resolution using
84 NiBabel (Brett et al., 2023), to allow each layer to be used as an ROI to interrogate each
85 qMRI image with statistical measures (e.g. median, standard deviation and kurtosis) across
86 the depth of the kidney. The gradient of the central layers can be calculated to estimate the
87 CMG in qMRI metrics. These metrics can be computed for the left and right kidney separately,
88 or analysis in a combined manner. Additionally, if the renal cortex and medulla ROIs are
89 available, the distribution of tissue types across layer depth can be explored. As the layers
90 are generated from a structural image rather than the quantitative map, using 3DQLayers
91 stipulates no requirements on quantitative map acquisition, unlike TLCO.

92 An object-oriented interface is provided to allow end users to simply generate layers and apply
93 these to qMR images. Documentation is provided to guide users through installation via PyPI,
94 conda or from source code on GitHub; it also includes tutorials and an API reference. An
95 automated test suite with high coverage provides users with confidence in the stability of
96 3DQLayers and that there will be no unexpected changes to results unless highlighted in the
97 change-log.

98 Usage Examples

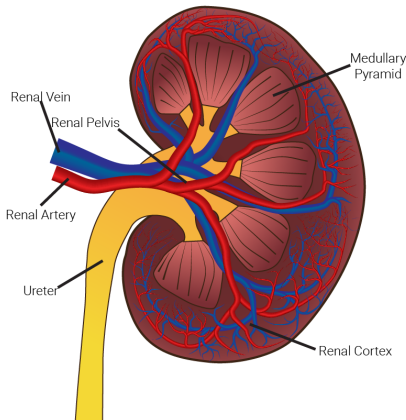
99 [Figure 3](#) shows the use of 3DQLayers to measure different gradients of R_2^* in a healthy volunteer
100 with normal renal function and a patient with impaired renal function (an estimated glomerular
101 filtration rate (eGFR) of above 90 ml/min/1.73m² measured from blood samples is considered
102 in the healthy range ([Stevens et al., 2006](#))). This replicates results shown using TLCO, with a
103 lower gradient in patients compared to healthies, however 3DQLayers controls for kidney size
104 resulting in the gradient being measured in quantitative units of Hz/mm rather than Hz/layer
105 as in TLCO, thus increasing generalisability.

106 [Figure 4](#) shows how 3DQLayers can be used in combination with cortex and medulla tissue ROIs
107 to analyse the distribution of voxel counts of each tissue as a function of layer depth of the
108 kidney. Here cortex and medulla ROIs are initially generated using a Gaussian mixture model to
109 segment a T₁-weighted structural image followed by manual ROI correction. From this, average
110 renal cortical thickness can be defined from the depth at which the voxel distribution crosses
111 from cortex to medulla. Cortical thickness has been hypothesised as a potential biomarker of
112 renal disease ([Yamashita et al., 2015](#)).

113 3DQLayers can also be used to analyse ex-vivo kidneys imaged outside the body. [Figure 5](#) shows
114 example quantitative maps acquired from a kidney removed for transplant but subsequently
115 deemed unsuitable and the associated layer profiles. [Figure 6](#) compares the results of tissue ROI
116 based analysis and layer-based analysis in fifteen transplant kidneys. A significant correlation
117 between outer layers and the cortex, and inner layers and the medulla was shown across all
118 quantitative mapping techniques and a significant correlation between cortico-medullary ratio
119 and layer gradient was shown for T₁, T₂, T₂^{*} and Magnetisation Transfer Ratio (MTR)
120 mapping.

121 **Figures**

a.



b.

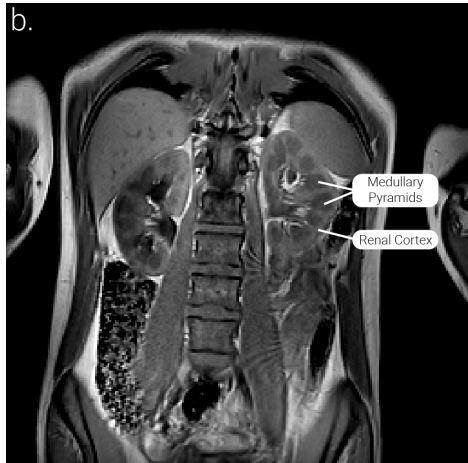


Figure 1: a) A schematic of the kidneys showing the renal cortex and medullary pyramids. b) A T₁-weighted structural MR image of the abdomen showing the kidneys with the renal cortex appearing as a light band on the outer edge of the kidney and the medullary pyramids as darker patches on the inner portion of the kidneys.

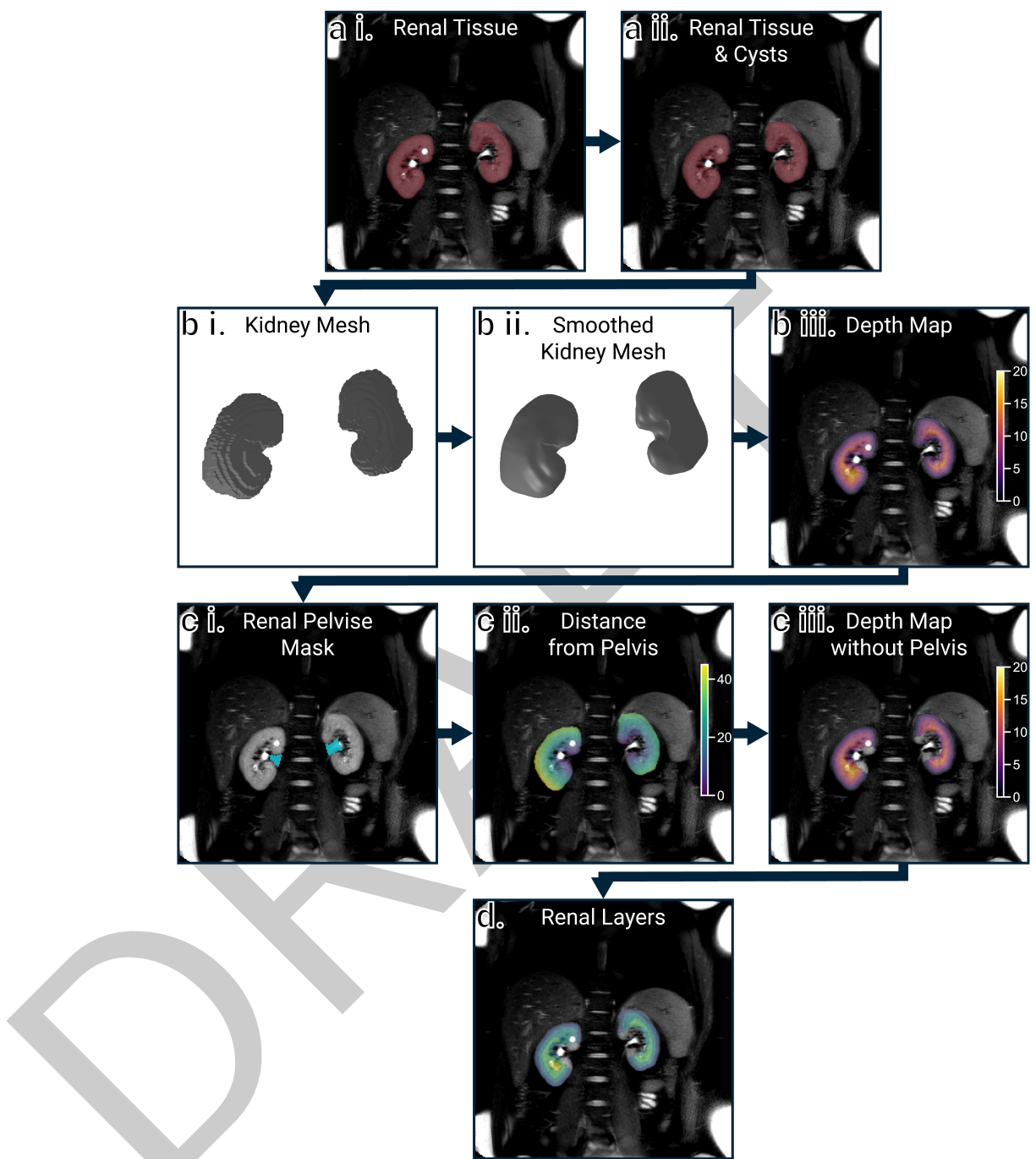


Figure 2: The mask automatically computed using a U-net from the T₂-weighted structural MR image (a i) has any cysts filled (a ii) and is converted into a smooth mesh representing the renal surface (b i and ii). The distance (in mm) of each voxel to the surface of the mesh is then calculated to generate a depth map (b iii). The renal pelvis is segmented (c i) and any tissue within 10 mm (c ii) of the pelvis is excluded from the depth map (c iii). The tissue is then grouped into layers of a desired thickness, here shown as 5 mm renal layers for illustrative purposes (d).

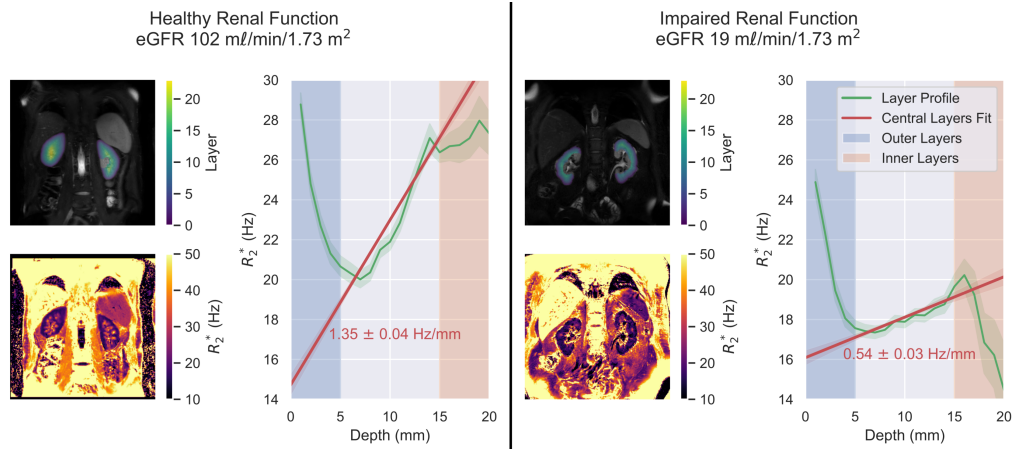


Figure 3: Layers, R_2^* maps, layer profiles, and central layer gradients for the left and right kidneys combined measured using 3DQLayers. Examples are shown for a subject with normal renal function and a patient with impaired renal function. Shading around profiles shows the 95% confidence interval within each layer.

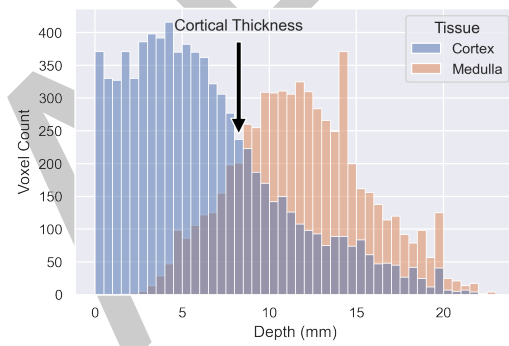


Figure 4: Exploring the distribution of tissue types through the kidney to measure cortical thickness.

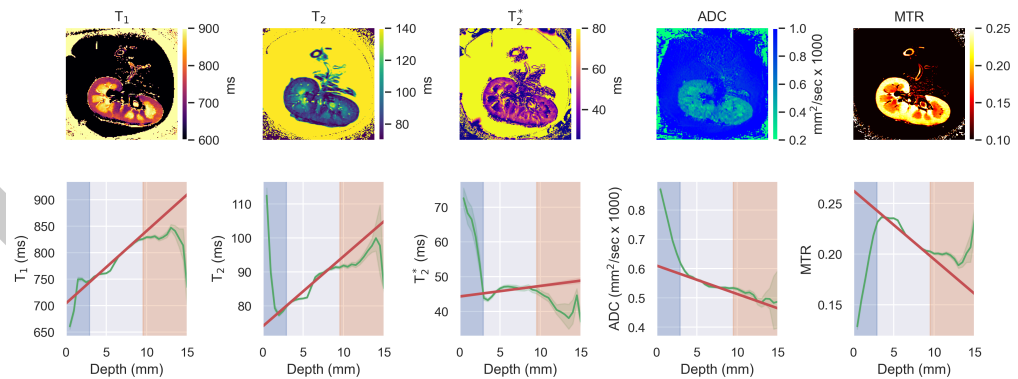


Figure 5: Example quantitative maps and associated layer profiles when 3DQLayers is applied to ex-vivo transplant kidneys. Uncertainty shading shows the 95% confidence interval of each layer.

Agreement between tissue ROI-based measures and analogous layer-based measures shown for fifteen ex-vivo transplant kidneys for each qMRI alongside the Pearson's correlation coefficient (ρ). * represents a p -value between 0.05 and 0.01, ** between 0.01 and 0.001, and *** < 0.001 . a) Plots the median within each tissue ROI (cortex or medulla semi-automatically defined) against the equivalent layers (outer layers and inner layers respectively as highlighted in Figure 5) b) Shows the cortico-medullary ratio (calculated by dividing the median within the cortex ROI by the median within the medullary ROI) against central layer gradient profiles calculated using 3DQLayers.

Figure 6: Agreement between tissue ROI-based measures and analogous layer-based measures shown for fifteen ex-vivo transplant kidneys for each qMRI alongside the Pearson's correlation coefficient (ρ). * represents a p -value between 0.05 and 0.01, ** between 0.01 and 0.001, and *** < 0.001 . a) Plots the median within each tissue ROI (cortex or medulla semi-automatically defined) against the equivalent layers (outer layers and inner layers respectively as highlighted in Figure 5) b) Shows the cortico-medullary ratio (calculated by dividing the median within the cortex ROI by the median within the medullary ROI) against central layer gradient profiles calculated using 3DQLayers.

122 Acknowledgements

123 We acknowledge the funding support of the ADMIRE project funded through Kidney Research
 124 UK (KS_RP_002_20210111), and the UKRIN_MAPS project funded by the Medical Research
 125 Council (MR/R02264X/1), as well as the NIHR Nottingham Biomedical Research Centre during
 126 the genesis of this project.

127 References

- 128 Bane, O., Mendichovszky, I. A., Milani, B., Dekkers, I. A., Deux, J.-F., Eckerbom, P., Grenier,
 129 N., Hall, M. E., Inoue, T., Laustsen, C., Lerman, L. O., Liu, C., Morrell, G., Pedersen,
 130 M., Pruijm, M., Sadowski, E. A., Seeliger, E., Sharma, K., Thoeny, H., ... Prasad, P. V.
 131 (2020). Consensus-based technical recommendations for clinical translation of renal BOLD
 132 MRI. *Magnetic Resonance Materials in Physics, Biology and Medicine*, 33(1), 199–215.
 133 <https://doi.org/10.1007/s10334-019-00802-x>
- 134 Bazin, P.-L., Weiss, M., Dinse, J., Schäfer, A., Trampel, R., & Turner, R. (2014). A
 135 computational framework for ultra-high resolution cortical segmentation at 7 Tesla.
 136 *NeuroImage*, 93, 201–209. <https://doi.org/10.1016/j.neuroimage.2013.03.077>
- 137 Brett, M., Markiewicz, C. J., Hanke, M., Côté, M.-A., Cipollini, B., McCarthy, P., Cheng, C.
 138 P., Halchenko, Y. O., Cottaar, M., Ghosh, S., Larson, E., Wassermann, D., Gerhard, S.,
 139 Lee, G. R., Kastman, E., Rokem, A., Madison, C., Morency, F. C., Moloney, B., ... freec84.
 140 (2023). NiBabel (Version 5.1.0). Zenodo. <https://doi.org/10.5281/zenodo.591597>
- 141 Daniel, A. J. (2024). *Renal Segmentor* (Version 1.3.9). <https://doi.org/10.5281/zenodo.4068850>
- 142 Daniel, A. J., Buchanan, C. E., Allcock, T., Scerri, D., Cox, E. F., Prestwich, B. L., & Francis,
 143 S. T. (2021). Automated renal segmentation in healthy and chronic kidney disease subjects
 144 using a convolutional neural network. *Magnetic Resonance in Medicine*, 86(2), 1125–1136.
 145 <https://doi.org/10.1002/mrm.28768>
- 146 Dawson-Haggerty, M. (2023). *Trimesh* (Version 4.0.0). <https://github.com/mikedh/trimesh>
- 147 Fischl, B. (2012). FreeSurfer. *NeuroImage*, 62(2), 774–781. <https://doi.org/10.1016/j.neuroimage.2012.01.021>
- 148 Goebel, R. (2012). BrainVoyager — Past, present, future. *NeuroImage*, 62(2), 748–756.
 149 <https://doi.org/10.1016/j.neuroimage.2012.01.083>

- 152 Hall, J. E. (2015). *Guyton and Hall Textbook of Medical Physiology*. Elsevier Health Sciences.
153 ISBN: 978-1-4557-7005-2
- 154 Huntenburg, J. M., Steele, C. J., & Bazin, P.-L. (2018). Nighres: Processing tools for high-
155 resolution neuroimaging. *GigaScience*, 7(7), giy082. <https://doi.org/10.1093/gigascience/giy082>
- 156 Huntenburg, J., Wagstyl, K., Steele, C., Funck, T., Bethlehem, R., Fouquet, O., Larrat, B.,
157 Borrell, V., & Bazin, P.-L. (2017). Laminar Python: Tools for cortical depth-resolved
158 analysis of high-resolution brain imaging data in Python. *Research Ideas and Outcomes*, 3,
159 e12346. <https://doi.org/10.3897/rio.3.e12346>
- 160 Ishikawa, M., Inoue, T., Kozawa, E., Okada, H., & Kobayashi, N. (2022). Framework for
161 estimating renal function using magnetic resonance imaging. *Journal of Medical Imaging*,
162 9(2), 024501. <https://doi.org/10.1117/1.JMI.9.2.024501>
- 163 Jenkinson, M., Beckmann, C. F., Behrens, T. E. J., Woolrich, M. W., & Smith, S. M. (2012).
164 FSL. *NeuroImage*, 62(2), 782–790. <https://doi.org/10.1016/j.neuroimage.2011.09.015>
- 165 Li, L.-P., Milani, B., Pruijm, M., Kohn, O., Sprague, S., Hack, B., & Prasad, P. (2020). Renal
166 BOLD MRI in patients with chronic kidney disease: Comparison of the semi-automated
167 twelve layer concentric objects (TLCO) and manual ROI methods. *Magnetic Resonance*
168 *Materials in Physics, Biology and Medicine*, 33(1), 113–120. <https://doi.org/10.1007/s10334-019-00808-5>
- 169 Lote, C. J. (2012). *Principles of Renal Physiology*. Springer Science & Business Media.
170 ISBN: 978-94-011-4086-7
- 171 Milani, B., Ansaloni, A., Sousa-Guimaraes, S., Vakilzadeh, N., Piskunowicz, M., Vogt, B.,
172 Stuber, M., Burnier, M., & Pruijm, M. (2017). Reduction of cortical oxygenation in
173 chronic kidney disease: Evidence obtained with a new analysis method of blood oxygenation
174 level-dependent magnetic resonance imaging. *Nephrology Dialysis Transplantation*, 32(12),
175 2097–2105. <https://doi.org/10.1093/ndt/gfw362>
- 176 Piskunowicz, M., Hofmann, L., Zuercher, E., Bassi, I., Milani, B., Stuber, M., Narkiewicz, K.,
177 Vogt, B., Burnier, M., & Pruijm, M. (2015). A new technique with high reproducibility
178 to estimate renal oxygenation using BOLD-MRI in chronic kidney disease. *Magnetic*
179 *Resonance Imaging*, 33(3), 253–261. <https://doi.org/10.1016/j.mri.2014.12.002>
- 180 Stevens, L. A., Coresh, J., Greene, T., & Levey, A. S. (2006). Assessing Kidney Function —
181 Measured and Estimated Glomerular Filtration Rate. *New England Journal of Medicine*,
182 354(23), 2473–2483. <https://doi.org/10.1056/NEJMra054415>
- 183 Yamashita, S. R., Atzingen, A. C. von, Iared, W., Bezerra, A. S. de A., Ammirati, A. L.,
184 Canziani, M. E. F., & D'Ippolito, G. (2015). Value of renal cortical thickness as a predictor
185 of renal function impairment in chronic renal disease patients. *Radiologia Brasileira*, 48(1),
186 12. <https://doi.org/10.1590/0100-3984.2014.0008>
- 187
- 188